

# Fuzzy Gradient Control of Electric Vehicles at Blended Braking with Volatile Driving Conditions

Valery Vodovozov<sup>1</sup><sup>a</sup>, Eduard Petlenkov<sup>2</sup><sup>b</sup>, Andrei Aksjonov<sup>3</sup><sup>c</sup> and Zoja Raud<sup>1</sup><sup>d</sup>

<sup>1</sup>*Department of Electrical Power Engineering and Mechatronics, Tallinn University of Technology, Ehitajate tee 5, Tallinn, Estonia*

<sup>2</sup>*Department of Computer Systems: Centre for Intelligent Systems, Tallinn University of Technology, Ehitajate tee 5, Tallinn, Estonia*

<sup>3</sup>*School of Electrical Engineering, Intelligent Robotics Group, Aalto University, Espoo, Finland*

**Keywords:** Electric Vehicle, Intelligent Transportation, Fuzzy Control, Modelling, Simulation, Energy Recovery, Hybrid Energy Source, Braking System.

**Abstract:** The paper is devoted to intelligent control of road electric vehicles aiming at reducing energy losses caused by traffic jams, changing velocity, and frequent start-stop modes of driving. A blended braking system is described that integrates both the friction and the electric braking strengths in volatile driving conditions, including gradual and emergency antilock braking. The vehicle model reflects multiple factors, such as air resistance, road slope, and variable friction factor. A new gradient control method recognizes unstable tire properties on changing road surfaces at different velocities. In the motor and battery model, the state of charge and electric current/voltage restrictions of the hybrid energy storage are taken into account. The braking torque, actuated by the Mamdani's fuzzy logic controller established in the Simulink<sup>®</sup> environment, is allocated between the front and rear friction and electric brakes. Comparison of simulation and experimental results confirms that the outcomes of this research can be considered in the design of braking systems for electric vehicles with superior energy recovery.


## 1 INTRODUCTION


In development of control systems for road electric vehicles, many novel energy saving trends are discovered nowadays. In view of the fact that up to 50 – 70% of vehicle energy is lost during deceleration (Shang et al., 2010; Savaresi et al., 2010), the braking energy recovery might reclaim this loss and extend driving range and time. Thereby, the introduction of modern blended braking systems has become a top priority and moves forward intensively in recent years. Such systems combine traditional friction braking (FB) with regenerative electric braking (EB) associated with hybrid energy storage machinery that unites both high energy density modules (batteries) and high power density blocks (ultracapacitors or/and flywheels) (Naseri et al., 2017). Blended braking has


attracted attention in science and industry because of reduced car maintenance costs and lowered tire particles emission, among others.


Most electric vehicle designers, such as (Chen et al., 2017; Xie and Wang 2018), prefers EB for vehicle gradual slowing down and FB for intensive deceleration. EB is commonly out of use in the antilock braking system (ABS) and is not applied as an urgent braking tool because the force generated by an electric motor is often quite small to produce the total braking torque needed to ensure a quick and steerable stop. Primarily, the EB fails due to battery overheating and the state-of-charge (SOC) restrictions of the energy storage.

When discussing the distribution of braking torque in blended braking systems, three approaches fall to the focus of attention: force assignment

<sup>a</sup> <https://orcid.org/0000-0002-5530-3813>

<sup>b</sup> <https://orcid.org/0000-0003-2167-6280>

<sup>c</sup> <https://orcid.org/0000-0001-7460-6548>

<sup>d</sup> <https://orcid.org/0000-0001-5197-3599>

between right and left wheels, power sharing among front and rear wheels, and torque allocation between EB and FB systems (Xu et al., 2016). The last issue is aimed at acquiring maximal braking energy from both EB and FB ensuring highest regeneration capacity and involving the EB to energy exchange in the best possible way (Xie and Wang, 2018). At that, the ABS occupies a special place and usually represents a separate part of the vehicle, since its primary target is to reduce the braking distance and time.

Usually, ABS performs poorly in volatile and unknown road conditions because of its focus on high-speed driving on straight dry roads. As a result, when rain, snow, or loose gravel appears, ABS can lengthen the braking distance and braking time instead of shortening them due to improper control organisation. To resolve the problem, intelligent ABSs with slip adjustment were proposed (Naseri et al., 2017; Chen et al., 2017).

For the systems that have non-linear and time variant plants with significant dead time, multiple fuzzy control approaches were published recently. Thanks to such universal approximator as a fuzzy logic controller (FLC), the most progressive of them, for instance (Givigi, 2010; Haidegger, 2011), successfully evaluate a priori unknown changes in the environment over time in order to understand the process and to find a solution of the dynamic differential or difference equations. In (Radgolchin, 2018), a fuzzy controller is designed to stabilize a moving plant at unknown deflections. The efficiency of this FLC is enhanced using a second level supervisory controller. The fuzzy algorithm proposed in (Precup, 2014) computes the control signal vector applied to the chaotic continuous-time dynamical system to ensure its stabilization.

In (Lin and Song, 2011), changes in the properties of tires, road surfaces, and vehicle deceleration can be estimated taking into account the displacement and rate of the brake pedal pressing, vehicle velocity, and wheel slip as the FLC input signals. Nevertheless, this specificity eliminates the use of EB in the ABS and separates the ABS from the general braking system. As a rule, while the braking intensity demand is small, EB is elected, but as the ABS is requested, FB is applied (Jing et al., 2011).

Just like in the initial part of this research published in (Aksjonov et al., 2018; Aksjonov et al., 2019), the current study is devoted to creating a hybrid energy-storage-oriented blended braking system suitable for different braking modes on various road surfaces and velocities. However, new factors are taken into account here aiming at improving the efficiency of energy recovery and the

versatility of the system. First, thanks to the torque gradient control, the available range of volatile driving conditions is expanded without losing the quality of braking. Second, in addition to ABS, the offered braking system can operate in both gradual and emergency braking modes. Third, in contrast to many known ABS, the quality of braking in this study does not depend on the initial vehicle velocity, air resistance, or road incline.

The problem of braking management is formulated as a search among three actions: urgent braking with fuzzy ABS control upon maximally possible EB involvement; gradual braking with greatest energy recovery; or non-electric braking. The research objective is to achieve the best energy recovery in the first two scenarios with minimal participation of the third one. The following five sections present the new braking system with gradient control, the vehicle friction model, the motor-battery model, and their operation. Then, the versatile braking FLC is designed. Next, the simulation is performed, the experimental diagrams are compared to the simulation outcomes, and the results obtained are summarized.

## 2 MODEL OF BRAKING SYSTEM

In compliance with (Reif, 2014; Kiyakli and Solmaz, 2018), dynamics of the braking single-wheel quarter-vehicle are determined as follows:

$$ma = F_B, \quad (1)$$

$$F_B = F_{air} + F_g + F_x, \quad (2)$$

$$F_{air} = 0.5\rho C_{air} Q (v_v + v_{wind})^2 \operatorname{sgn}(v_v + v_{wind}), \quad (3)$$

$$F_g = mg \sin(\beta), \quad (4)$$

$$F_x = \mu mg \cos(\beta), \quad (5)$$

$$T_B = F_B r + J \frac{d\omega_w}{dt}, \quad (6)$$

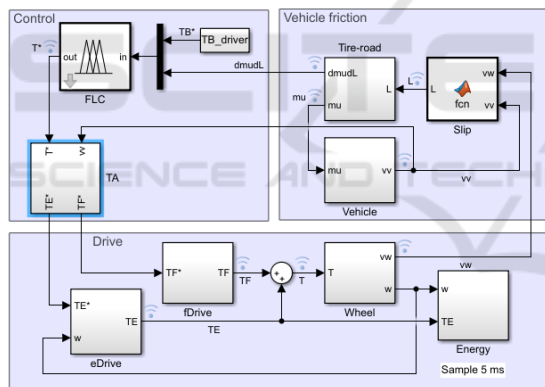
where

- $m$  – quarter-vehicle mass;
- $a$  – longitudinal deceleration of vehicle;
- $F_B$  – braking force;
- $F_{air}$  – air resistance (aerodynamic drag);
- $\rho$  – air density;
- $C_{air}$  – aerodynamic drag coefficient;
- $Q$  – vehicle front area;
- $v_v$  – vehicle velocity;
- $v_{wind}$  – wind velocity;

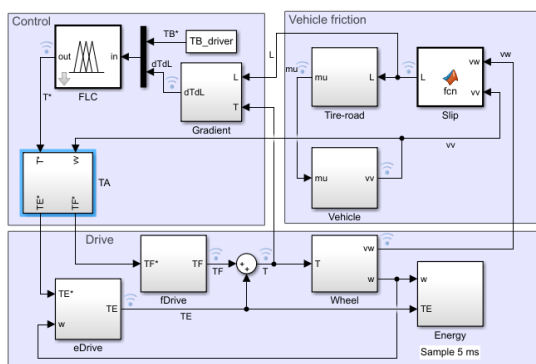
- $F_g$  – climbing force;
- $g$  – acceleration due to gravity;
- $\beta$  – climbing slope (road incline);
- $F_x$  – longitudinal force;
- $\mu$  – dimensionless friction factor;
- $T_B$  – braking torque;
- $r$  – effective radius of the wheel;
- $\omega_w$  – angular speed of the wheel;
- $J$  – moment of inertia of the wheel.

Two variants of the explored Simulink® model of blended braking with fuzzy gradient control are shown in Fig. 1: the friction-slip system (a) and the torque-slip system (b). They are made up of the following groups of blocks:

- *Vehicle friction* group including *Tire-road*, *Slip*, and *Vehicle* blocks;
- *Drive* group, including electric drive (*eDrive*), friction drive (*fDrive*), *Wheel*, and *Energy* blocks;
- *Control* group, including the fuzzy logic controller (*FLC*) and torque allocation (*TA*) blocks. The FLC derives an actuating braking torque  $T^*$  for vehicle deceleration using the velocity and tire-road (a) or application torque (b) gradient signals.



(a)



(b)

Figure 1: Simulink® models of the blended braking system with friction-slip (a) and torque-slip (b) gradient control.

### 3 WHEEL SLIP AND TIRE-ROAD FRICTION ESTIMATES

To slow down the vehicle moving at certain initial velocity  $v_0$ , the required braking force  $F_B$  has to be developed. To this aim, the control system needs the data used in Eqs. (1) – (6). Most of them are available from the vehicle passport characteristics ( $m, Q, r, J$ ) or can be acquired with on-board sensors ( $a, v_v, v_{winds}, \omega_w$ ).

However, estimating the total tire-road friction is a complex challenge since this parameter varies with such factors as velocity, load, torque, surface roughness, tire diameter, inflation, wear, etc., and these variations are very difficult to detect. Moreover, the friction depends on the wheel slip.

Unlike the graduate braking, in intensive braking a longitudinal wheel slip  $\lambda$  takes place (Reif, 2014; Spichartz et al., 2017) i.e. the relative difference between vehicle ( $v_v$ ) and wheel ( $v_w$ ) velocities:

$$\lambda = \frac{v_v - v_w}{v_v} = \frac{v_v - \omega_w r}{v_v}. \quad (7)$$

This means that in addition to minor rolling friction, slipping friction heavily affects the braking rate. It involves both the kinetic interaction of moving surfaces, called sliding or dynamic friction, and the static coupling (“stiction”) of fixed surfaces. The latter one significantly exceeds its kinetic counterpart at the beginning of starting and at the end of braking. The force that prevents a tire from slipping as it rolls on the ground is an example of static friction. Even though the wheel is in motion, the patch of the tire that contacts the ground is stationary relative to the ground, so it is a static rather than a kinetic friction (Pratap and Ruina, 2002).

To derive the wheel slip in real time, both velocities in Eq. (7) can be directly measured with on-board  $v_v$  and  $\omega_w$  sensors. However, since the friction cannot be acquired by sensors, one or the other computational method is required for its estimation.

The knowledge of the friction-slip characteristics  $\mu(\lambda, v_v)$  is needed not only to ensure the anti-spin regulation and antilock braking, but also, for adaptive cruise control and energy recovery. As direct friction sensing is impossible, many studies devoted to its indirect estimation have been produced aiming to arrange the braking procedure. In all cases, some forms of the model-based approach are used for  $\mu(\lambda, v_v)$  searching. In (Zhang and Lin 2018), friction is derived based on velocity sensor signals and vehicle geometry. In (Kadowaki et al., 2007), a

perturbed sliding mode observer is used. Several models of the friction-slip relations may be found in literature, such as Pacejka’s “Magic Formula”, Burekhardt model, Rill model, and others (Cecotti, 2012).

Although the factors in these models are different, the trends of curves look very similar. Commonly, the tire-road friction factor grows steeply from zero to its maximum appeared somewhere between 2 and 12% slip for different road surfaces. At 0% slip, both the wheel and the vehicle have exactly the same velocities in Eq. (7). Gradual braking operations presume low levels of slip and take place within a zone where an increase in the slip simultaneously produces an increase in the usable friction. These growing slopes of the friction-slip characteristics match the stable zone where, due to the positive friction-slip gradient, the vehicle is suitable for control and for steerability maintenance. On the contrary, the falling slopes emphasise an unstable zone, in which the wheels may lock up, inducing skidding and causing the spinning of the tires. When the slip is 100%, the wheel is locked although the vehicle is still moving.

In this research, a programmable road estimator was implemented in the *Tire-road* block shown in Fig. 1, where a preliminary stored set of friction-slip lookup tables is used. Its input is associated with the *Slip* block and vehicle deceleration  $a$  is derived from the ratio of the longitudinal ( $F_x$ ) and normal ( $F_z$ ) forces acting on the wheel:

$$\mu(\lambda, v_v) = \frac{F_x}{F_z} = \frac{ma - F_{air} - F_g}{mg \cos(\beta)} \quad (8)$$

Further, vehicle velocity is counted by integrating  $a$  as shown in Fig. 2, where it is assumed that  $F_{air} = \beta = 0$  with a view to simplicity.

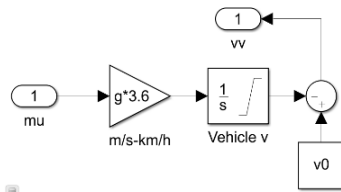


Figure 2: The *Vehicle* block.

Naturally, given the very large uncertainty associated with the above estimates due to incomplete data, this approach does not claim to be highly accurate. As the velocity decreases, the curves tend to move down and right, meaning that the dynamics of the wheel slip is inversely proportional to the vehicle velocity (Habibi and Yazdizadeh, 2010; Cerdeira-

Corujo et al., 2016; Li et al., 2018). Additionally, such tire properties as their type, inflating pressure, etc. also change during braking, affecting their peak locations. An important challenge is to identify the changing road surface in order to select the proper  $\mu(\lambda, v_v)$  characteristic.

## 4 GRADIENT CONTROL METHOD

In contrast to (Aksjonov et al., 2018), where the acceleration signal is sent directly to the controller, in the new model presented in Fig. 1 this signal is only needed to estimate the vehicle velocity in the *Vehicle* block.

To reduce the uncertainty of the friction characteristics, the steerable braking condition can be confidently expressed as

$$\frac{d\mu}{d\lambda} \geq 0. \quad (9)$$

In accordance with Eq. (9), the fastest braking process is expected at the maximal braking force  $F_B$  corresponding to  $\frac{d\mu}{d\lambda} = 0$ .

In the model of Fig. 1-(a), the desired friction factor and the measured slip ratio are used in the same *Tire-road* block to determine how great force can be created in response to an increase of wheel slip.

Estimation of Eq. (9) in real time is based on the tire model Eq. (8). Two approaches are proposed to overcome differentiation noise. In the first case, a filtering technique (Cecotti et al., 2012) is adopted. As the second method, pre-calculated friction derivatives are collected in the lookup tables to be used instead of real-time differentiation. The gradient obtained by any of these approaches is further directed to the control system.

Both techniques are illustrated in Fig. 3, where two lookup tables keep data on the friction-slip ( $\mu$ - $L$ ) relations on wet ( $\mu_{wet}$ ) and dry ( $\mu_{dry}$ ) roads, and two other lookup tables ( $d\mu_{L\_wet}$  and  $d\mu_{L\_dry}$ ) keep data on the pre-calculated gradients. The signals about the change of the road surface connect the appropriate tables to the outputs of the block. At that, the derivatives are restricted according to the universe of discourse (UOD) of the connected controller.

Management of braking using Eq. (9) is called further a friction-slip gradient control. Since friction cannot be sensed directly and this control approach

remains fairly rough, the estimated tire-road friction factor is to be taken with a margin relative to its maximum. As a result, this system does not claim any significant advantages over (Aksjonov et al., 2018).

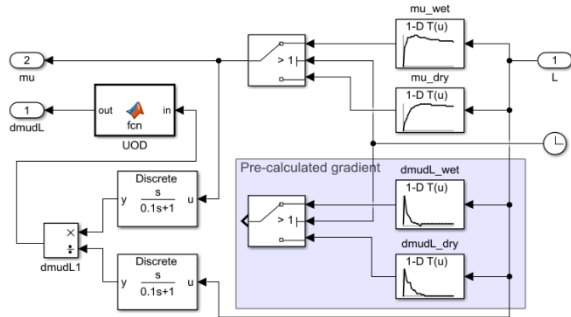


Figure 3: The Tire-road block.

However, as a development of this approach, a more advanced method is further proposed.

Assuming that  $J \frac{d\omega_w}{dt}$  remains rather constant in the controller computational interval, Eq. (6) can be converted as

$$\frac{dT_B}{d\lambda} = r \frac{dF_x}{d\lambda} = k \frac{d\mu}{d\lambda}, \quad (10)$$

where  $k = mgr \cos(\beta)$ .

In turn, since at the steerable braking the torque  $T_B$  follows the application torque  $T$  of the drive, Eq. (9) is re-written as follows:

$$\frac{d\mu}{d\lambda} = \frac{1}{k} \frac{dT}{d\lambda} \geq 0. \quad (11)$$

Now, the derivative of application torque with respect to slip may be used as a control feedback. It is called further a torque-slip gradient control.

Whereas the application torque is easily measured with sensors and accurately adjusted (Xu et al., 2016), the torque-gradient control represents a kind of the close loop control. In this way, vehicle velocity, particularly at statics, as well as other road, aerodynamics, and incline features are successfully considered into the tire model as was recommended in (Habibi and Yazdzizadeh, 2010; Cecotti et al., 2012).

The torque-slip gradient control is illustrated in Fig. 1-(b) and Fig. 4, where the Gradient block implements differentiation of measured application torque  $T$ , whereas the Tire-road block is only needed for estimating the friction using data from the Slip block fed by the on-board  $v$  and  $\omega_w$  sensors.

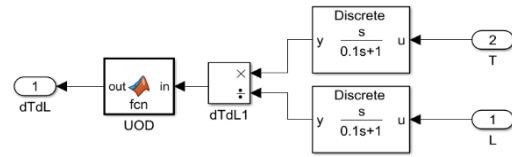


Figure 4: The Gradient block.

## 5 DRIVE MODEL

In the Drive group, the friction drive  $fDrive$  block, integrated with FB, and the adjustable electric drive  $eDrive$  block, implemented the battery-regenerative EB, handle separately their portions of the actuating braking torque  $T^*$  generated by the Control group.

The FB unit is modelled as a first order system with dead time.

In turn, the Drive-U sub-block in  $eDrive$  (Fig. 5) is responsible for direct torque control, electrical power supply, and energy recovery. Together with the Drive-I sub-block, it arranges a torque stabilisation loop with PI current controller.

The Drive-T sub-block and the Wheel block belong to the speed loop activated in gradual deceleration and shorted in emergency braking.

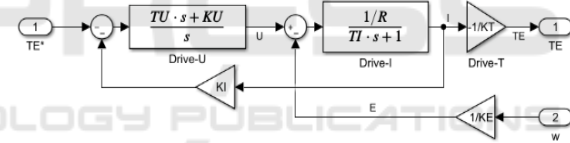


Figure 5: The eDrive block.

Gear and vehicle inertia are represented by the Wheel block also (Fig. 6). The static fraction of torque is taken into account in this model when the velocity drops to a low ( $v_{home}$ ) level.

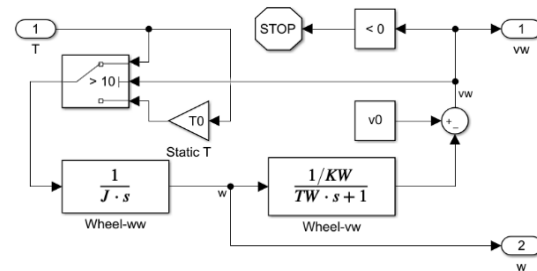


Figure 6: The Wheel block.

The Energy block (Fig. 7) derives an electrical fraction of the braking power

$$P_E = T_E \omega_w \quad (12)$$



and braking energy regenerated back to the supply grid with efficiency  $\eta$  in a given time interval  $t$ :

$$W_E = \eta \int P_E dt \quad (13)$$

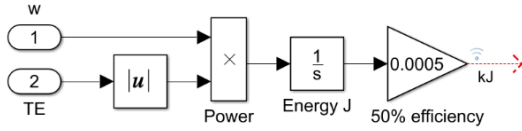


Figure 7: The Energy block.

## 6 TORQUE ALLOCATION

The main mission of the blended braking system is to slow down a vehicle under the action of the application torque  $T$ , which should be as close as possible to the driver's setpoint  $T_B^*$  (the block  $TB\_driver$  in Fig. 1), without exceeding peak optimality for the road surface under the tires.

The *Control* group generates actuating braking torque  $T^*$  dependently of the pedal displacement  $T_B^*$  and friction gradient  $d\mu/d\lambda$  (Fig. 1-(a)) or application torque gradient  $dT/d\lambda$  (Fig. 1-(b)). Its output torque allocation block ( $TA$ ) algorithmically distributes the actuating braking torque  $T^*$  between the front and rear wheels in a fixed ratio (Tao et al., 2017) and allocates it between FB and EB based on real-time SOC, voltage, and permissible EB current. Electric current  $I_E$  recharges the energy storage device from the EB while the pressure signal  $p_F$  adjusts the FB. Braking will complete when the driver releases the pedal or the vehicle stops.

In order to forward to EB a maximal fraction of the actuating torque  $T^*$ , the electric drive has to develop sufficient power, voltage, and current to charge all energy storage devices:

$$\begin{aligned} P_{E \max} &> \max(P_{UC \max}, P_{BAT \max}) \\ U_{E \max} &> \max(U_{UC \max}, U_{BAT \max}), \\ I_{E \max} &> \max(I_{UC \max}, I_{BAT \max}) \end{aligned} \quad (14)$$

where  $P_{UC \max}$ ,  $U_{UC \max}$ ,  $I_{UC \max}$ ,  $P_{BAT \max}$ ,  $U_{BAT \max}$ , and  $I_{BAT \max}$  are permissible power, voltage, and current of the ultracapacitor (UC) and the battery (BAT), respectively;  $P_{E \max}$ ,  $U_{E \max}$ , and  $I_{E \max}$  – maximal power, voltage, and current of the electric drive.

Meanwhile, in order to keep the battery and ultracapacitor within their safe operating areas, electric current  $I_E$  and motor torque  $T_E^*$  have to meet the real-time storage restrictions, namely,  $SOC_{UC}$  and  $SOC_{BAT}$  (Cerdeira-Corujo, 2016; Naseri et al., 2017):

$$\begin{aligned} T_E^* &= I_E \psi = \\ \max & [I_{UC}(SOC_{UC})\psi, I_{BAT}(SOC_{BAT})\psi] \end{aligned} \quad (15)$$

where  $I_{UC}$  and  $I_{BAT}$  are estimated charging currents of the ultracapacitor and battery and  $\psi$  is flux linkage of the electric motor.

Once the actuating braking torque exceeds these boundaries, the remaining part of it must be created by the FB:

$$T_F^* = T^* - T_E^* \quad (16)$$

In (Aksjonov et al., 2019), an appropriate torque allocation algorithm is proposed. There, when the control system recognises the actuating torque request  $T^*$ , the EB is activated and either  $EB_{UC}$  or  $EB_{BAT}$  runs. The FB torque does not appear until either any of the SOC levels exceeds the allowed overcharging barriers or the electric motor produces maximal power. As soon as the motor torque becomes insufficient, the system runs FB and EB together. Only in the case when both SOC levels exceed their boundaries, the solo FB is used due to the inability to regenerate.

Therefore, the common trait of this strategy is to include regeneration into all braking scenarios, even during heavy braking with ABS, and to use the solo FB only when the battery SOC and voltage levels are saturated. The fewer such conditions appear, the less braking energy is wasted and the longer the service life of the FB.

## 7 DESIGN OF A FUZZY LOGIC CONTROLLER

Depending on the solution chosen, the fuzzy (Tao et al., 2017), PID (Cerdeira-Corujo et al., 2016; Kiyakli and Solmaz, 2018), sliding (Kadowaki et al., 2007; Habibi and Yazdizadeh, 2010), and some other braking controllers compete in the market. Given the complexity of the system and its nonlinearity, this study is devoted to the FLC relying on the knowledge and skills of professional experts.

The FLC target is to derive an actuating braking torque  $T^*$  needed for slowing down the vehicle inside an acceptable friction-slip region. In the MISO-type controller designed, two input numerical variables (crisps) are used: the driver's setpoint  $T_B^*$  and either the friction ( $d\mu/d\lambda$ ) or the application torque ( $dT/d\lambda$ ) derivative with respect to slip  $\lambda$ .

The Mamdani-style inference mechanism is applied to transform every input crisp into a separate fuzzy pair consisting of an element in UOD and an

appropriate membership function (MF). The estimated actuating torque  $T^*$  is coming from the FLC output. Using the weighted average defuzzification method, this linguistic signal is then turned back to the real-world output crisp.

The setpoint torque input  $T_B^*$ , the gradient input  $dT/d\lambda$  (or  $d\mu/d\lambda$ ), and the actuating torque  $T^*$  output have six MFs notated as Z (Zero), VS (Very Small), S (Small), M (Middle), B (Big), and VB (Very Big).

In Fig. 8, the fuzzy sets for the linguistic variables are represented. The MFs have a triangle shape suitable for braking management and experts training.

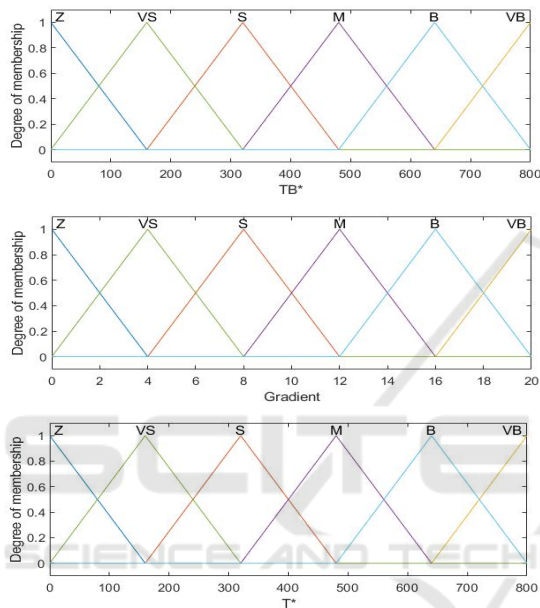


Figure 8: MFs of control variables  $T_B^*$ , Gradient, and  $T^*$ .

The inference engine with “If-Then” modulus ponens converts fuzzy input sets to the fuzzy output set using the base of 36 rules shown in Table I.

Table 1: FLC Rule Base.

Gradient $d\mu/d\lambda, dT/d\lambda$	Output torque $T^*$ at input $T_B^*$					
	Z	VS	S	M	B	VB
Z	Z	Z	Z	Z	Z	Z
VS	Z	VS	VS	VS	VS	VS
S	Z	VS	S	S	S	S
M	Z	VS	S	M	M	M
B	Z	VS	S	M	B	B
VB	Z	VS	S	M	B	VB

The input-output FLC surface is plotted in Fig. 9.

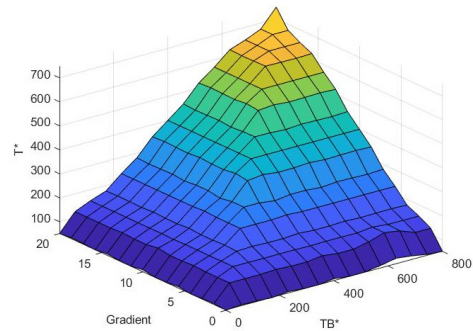


Figure 9: Input-output FLC surface.

## 8 EXPERIMENTATION

To validate the model described in the previous sections, the simulations are compared further to experimental results published in (Aksjonov et al., 2019).

The hardware-in-the-loop electro-hydraulic testbed from ZF TRW Automotive (Koblenz, Germany) granted for experimentation by TU Ilmenau (Germany) and driven by the vehicle-oriented software IPG CarMaker® (Karlsruhe, Germany) was used there. The detailed stand specification is given in (Aksjonov et al., 2019). Its tire-road model based on “Magic Formula” (Pacejka, 2012) was parameterized against the real sport utility vehicle and represented as a table of friction-slip data under the fixed load on the wheels and the most common road surfaces (i.e., icy, wet, damp and dry). The peaks of the friction curves for each road surface are marked with dots in Fig. 10.

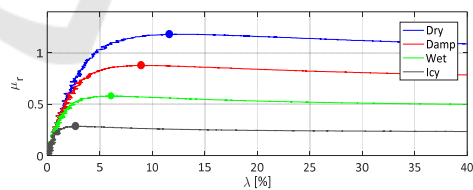


Figure 10: Tire-road friction factor plots for different road surfaces used in this study.

The weight of the studied sport utility vehicle is 2117 kg and wheel radius is 0.2 m. It was assumed that the vehicle is moving in a straight-line manoeuvre at 100 km/h, fed by the switch-reluctance motor with a maximal permissible torque of 200 Nm, speed 157 rad/s, and 2.1 kgm<sup>2</sup> inertia, connected to the wheel imitator through the gear of 10.5 ratio. Due to this transmission, the peak torque on the wheel at heavy braking can approach 2000 Nm, and the angular speed of the wheel – 15 rad/s. Aerodynamic

and climbing factors were neglected in that study ( $F_{air} = \beta = 0$ ).

In Fig. 11, the braking diagrams obtained in (Aksjonov et al., 2018) and confirmed experimentally in (Aksjonov et al., 2019) are shown. They demonstrate the velocities of the front left (*FL*), front right (*FR*), rear left (*RL*), and rear right (*RR*) wheels, appropriately, that follow the vehicle longitudinal velocity in Fig. 11-(a), and EB and FB wheel torque curves in Fig. 11-(b). Since the EB torque is not sufficient to retain optimal slip, the control system requests additional FB torque. At the end of slowing down, regeneration turns off, and the FB completes braking alone.

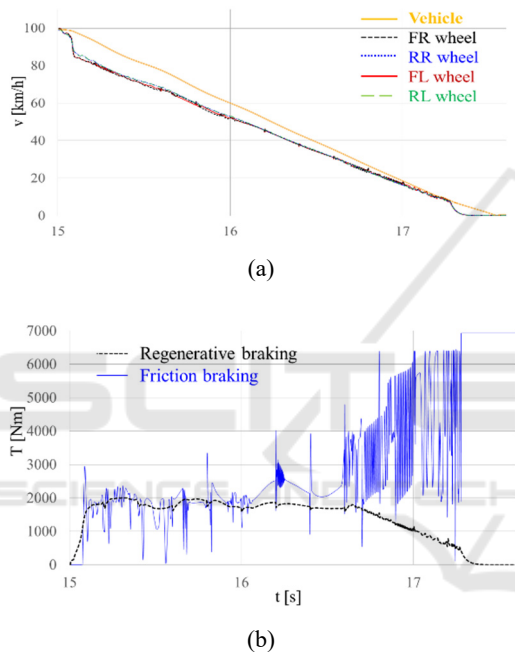


Figure 11: Experimental braking diagrams: (a) vehicle and wheel velocities; (b) torque.

An original method was proposed in (Aksjonov et al., 2018) for determining the road surface. Every second, starting from ABS activation, the controller evaluates the maximal deceleration of the vehicle and compares it with the deceleration peaks preliminary calculated using Eq. (8) at  $F_{air} = \beta = 0$ . Such momentary friction reset does not affect driving comfort, as the process is very rapid, but it indicates whether the road surface changes or remains the same as before.

Alongside the set of positive outcomes, the neglect of air friction, road slope, and other tire features are the drawbacks of the above method. As well, an evident chattering phenomenon at low velocity is seen in the torque plots. In fact, its

appearance can be explained by three interrelated reasons. First, this is an increase in static friction in Eq. (5), when the vehicle is moving slowly and several wheels tends to slip. Second, this is due to high sensitivity of the slip to the velocity at slow motion. Third, since at low velocity the EB ceases and the FB finalises braking alone, there is no torque stabilisation at that moment.

Torque oscillations demonstrate that the simplified drive model used could not ensure proper torque adjustment. Such kind of oscillation, reported also by other researchers (Habibi and Yazdizadeh, 2010; Lin and Song, 2011; Li et al., 2018) is a common issue of braking, needed to be considered as it affects vehicle steerability and reduces energy recovery.

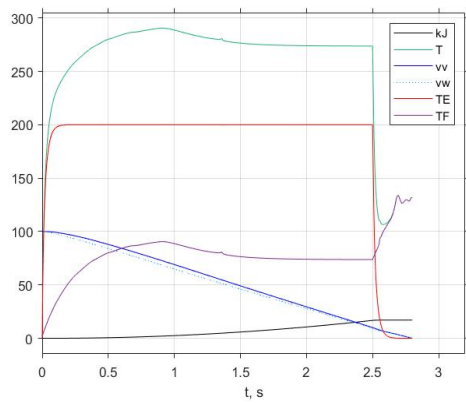
## 9 COMPARING SIMULATIONS TO EXPERIMENTAL RESULTS

The torque gradient approach proposed in the current research brings sensitive benefits in braking performance. Now, thanks to the close loop torque control, there is no longer need to collect theoretical tire-road friction data and determine the road surface. Appropriate simulation diagrams plotted for the same braking conditions as in (Aksjonov et al., 2019) confirm these advantages. Since the optimal wheel slip is approximately the same for both the front and the rear left and right wheels, a quarter-vehicle model described by Eqs. (1) – (6) is studied further.

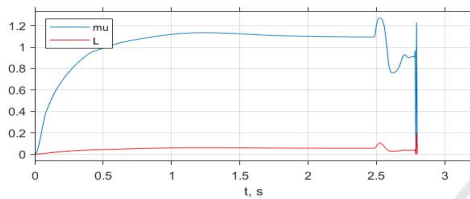
Figure 12 introduces the traces obtained from the friction-slip gradient control simulation. Here, the total application torque ( $T$ , green) needed to ensure intensive stopping in response to the driver's setpoint  $T_B^* = 270$  Nm is obtained after allocation between the electric ( $T_E$ , purple) and friction ( $T_F$ , violet) torques, wherein the electric torque is restricted to 200 Nm. Since the motor response is much faster than that of the friction unit,  $T_E$  can be considered almost the same as the demanded  $T_E^*$  unless it exceeds the limitation of the maximal electric power. Torque oscillations are not observed here as they are damped by the torque loop. At low velocity  $v_{home} = 10$  km/h, the friction increases sharply due to its static friction. The EB turns off, and the torque begins fluctuate intensely.

Figure 13 confirms the effectiveness of the torque-slip gradient control. Despite the fact that the braking process lasts here 10% longer due to the application torque delay and instability, the traces look very similar to Fig. 12.



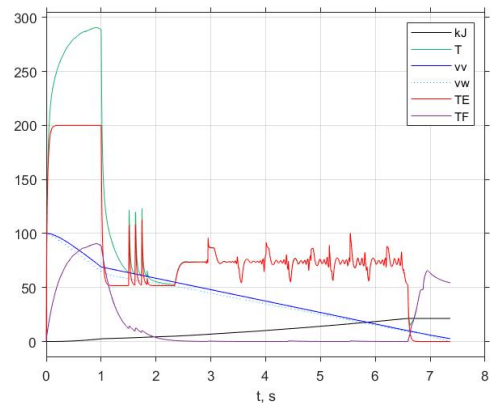


(a)

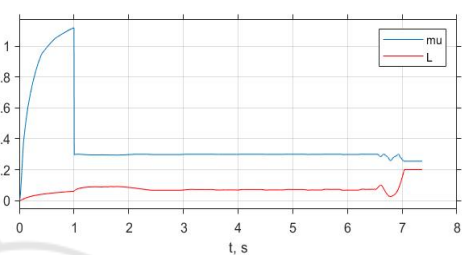


(b)

Figure 12: Friction-slip gradient braking diagrams at constant tire-road friction: (a) – vehicle and wheel velocities, electric, friction, and application torque, and regenerative energy; (b) – tire-road friction and wheel slip.

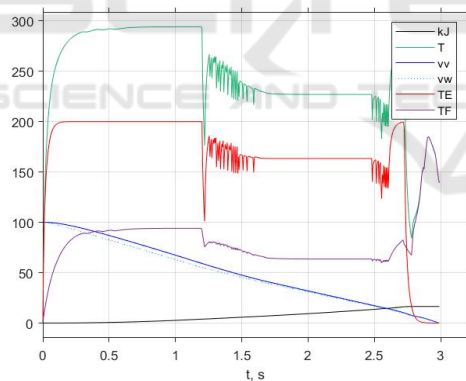


(a)

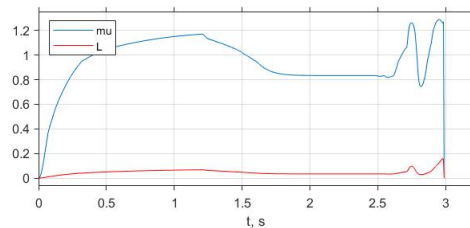


(b)

Figure 14: Friction-slip gradient braking diagrams at changing tire-road friction: (a) – vehicle and wheel velocities, electric, friction, and application torque, and regenerative energy; (b) – tire-road friction and wheel slip.



(a)



(b)

Figure 13: Torque-slip gradient braking diagrams at constant tire-road friction: (a) – vehicle and wheel velocities, electric, friction and application torque, and regenerative energy; (b) – tire-road friction and wheel slip.

In order to investigate the effectiveness of the proposed method in tracking more sophisticated commands, vehicle motion above the changing road surface was simulated. Figure 14 demonstrates the traces obtained from the simulation of the volatile driving using the friction-slip gradient control. Here, the system successfully detects a change in road conditions based on analysis of the friction-slip gradient. At the beginning, the deceleration was around  $20 \text{ m/s}^2$  on a dry surface. At the end of the first second, the road surface suddenly changes from dry to wet. As the new gradient is recognized, the total application torque needed to ensure an intensive stop drops to  $70 \text{ Nm}$ . The FB is no longer requested because the electric torque is sufficient to decelerate the vehicle within the optimal wheel slip area. Therefore, only electric braking is produced further. However, when the speed drops below  $v_{home}$ , the EB turns off, friction braking resumes and the FB operates alone.

Finally, Fig. 15 confirms the effectiveness of the torque-slip gradient control at the volatile driving. It represents the similar processes that take about 10% longer braking time.

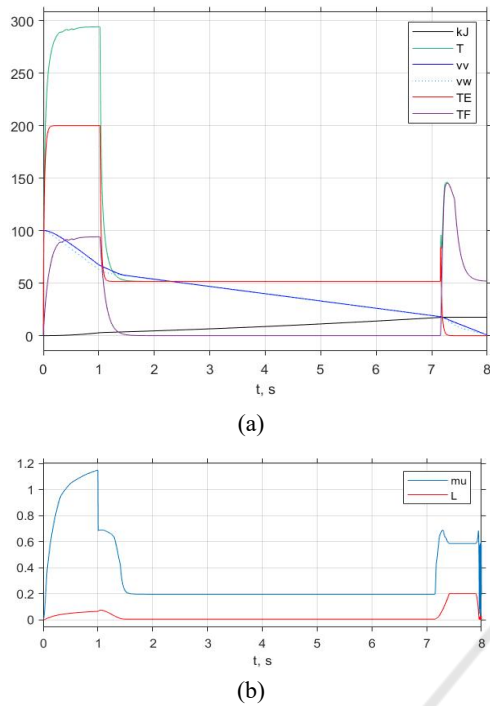


Figure 15: Torque-slip gradient braking diagrams at changing tire-road friction: (a) – vehicle and wheel velocities, electric, friction, and application torque, and regenerative energy; (b) – tire-road friction and wheel slip.

Herewith, there is no more chattering in the torque plots at low velocity. First, this is because the *Wheel* block takes into account an increase of friction due to its static friction. Second, because the air friction is involved in a close torque loop. Third and finally, because the torque loop remains closed even without the EB.

### 10 ANALYSIS OF ENERGY RECOVERY

Based on the energy curves (*kJ*, black) and assuming a 50% regenerative efficiency in Eq. (13), it turns out from Figs. 12-(a) and 13-(a) that nearly 22 kJ of energy is recovered during braking on the dry road. In Figs. 14-(a) and 15-(a), despite the fact that the stopping time is slightly increased, approximately the same amount of energy is recovered as before.

To assess the degree of involvement of aerodynamic and climbing resistances in energy consumption and saving, simulation were performed on the flat and 20°-downhill roads with different velocities. An electric car with  $Q = 3 \text{ m}^2$ ,  $\rho = 1.2 \text{ kg/m}^3$ , and  $C_{air} = 0.5$  was studied in the modes of gradual ( $\mu = 0.18$ ) and intensive ( $\mu = 1$ ) braking.

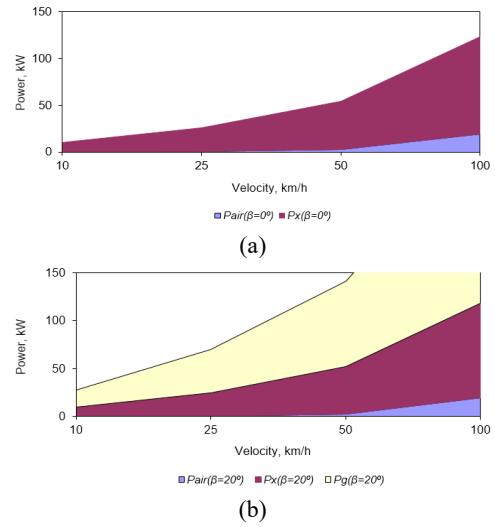


Figure 16: Power components at gradual braking,  $\mu = 0.18$ : (a)  $\beta = 0$ ; (b)  $\beta = 20^\circ$ .

At gradual braking without inclination ( $\beta = 0$  in Fig. 16-(a)), the friction power ( $P_x$ ) dominates only at low velocity, whereas in rapid cruising a significant part of energy is spent on overcoming the air resistance ( $P_{air}$ ). On the slope ( $\beta = 20^\circ$  in Fig. 16-(b)), much recovered energy can be released due to the climbing counterforce ( $P_g$ ). At heavy braking, the friction force ( $P_x$ ) always prevails on both the longitudinal (Fig. 17-(a)) and inclined (Fig. 17-(b)) driveways. However, until the friction factor reaches its upper level, it passes all intermediate levels, from 0.18 to 1, and all velocities, from  $v_0$  to 0. This means that both the volatile vehicle velocity and variable friction must be taken into account in braking control.

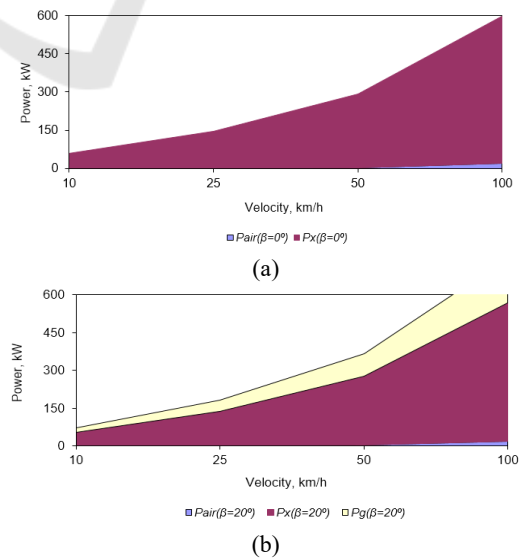


Figure 17: Power components at heavy braking,  $\mu = 1$ : (a)  $\beta = 0$ ; (b)  $\beta = 20^\circ$ .

## 11 CONCLUSION

In the refined vehicle model, multiple factors are addressed, such as air resistance, road slope, and changeable friction. An improved motor and energy source model reflects the state of charge and electric current/voltage restrictions of the hybrid energy storage under various driving scenarios recognised by the tire-road model, such as gradual deceleration and emergency antilock braking in volatile driving conditions. As a result, a proposed novel control arrangement provides fuzzy adjustment and stabilisation of the braking torque with a gradient torque allocation between electric and friction brakes, which allows integrating the advantages of both friction and electric braking. Obtained simulation diagrams largely coincide with the experimental curves. They demonstrate consistently high braking quality regardless of changes in the road surface and slope, vehicle initial velocity, and air resistance.

## ACKNOWLEDGEMENT

This work was supported by the Estonian Research Council grant PRG658.

## REFERENCES

- Aksjonov, A., Vodovozov, V., Augsborg, K. and Petlenkov, E., 2018. Design of regenerative anti-lock braking system controller for 4 in-wheel-motor drive electric vehicle with road surface estimation. *International Journal of Automotive Technology*, 19(4):727 – 742.
- Aksjonov, A., Vodovozov, V., Augsborg, K. and Petlenkov, E., 2019. Blended antilock braking system control method for all-wheel drive electric sport utility vehicle. In *ELECTRIMACS'19, 13th International Conference of the IMACS TCI Committee*, Salerno, Italy, pages 1 – 6.
- Cecotti, M., Larminie, J. and Azzopardi, B., 2012. Estimation of slip ratio and road characteristics by adding perturbation to the input torque. In *ICVES'12, IEEE International Conference on Vehicular Electronics and Safety*, Istanbul, Turkey, pages 31 – 36.
- Cordeira-Corujo, M., Costas, A., Delgado, E., Barreiro, A. and Banos, A., 2016. Gain-scheduled wheel slip reset control in automotive brake systems. In *SPEEDAM'16, International Symposium on Power Electronics, Electrical Drives, Automation and Motion*, Anacapri, Italy, pages 1255 – 1260.
- Chen, Z., Lv, T., Guo, N., Shen, J., Xiao, R., Lu, X. and Yu, Z., 2017. Study on braking energy recovery efficiency of electric vehicles equipped with super capacitor. In *CAC'17, Chinese Automation Congress*, Jinan, China, pages 7231 – 7236.
- Givigi Jr, S. N., Schwartz, H. M. and Lu, X. 2010. A reinforcement learning adaptive fuzzy controller for differential games. *Journal of Intelligent and Robotic Systems*, 59(1):3 – 30.
- Habibi, M. and Yazdizadeh, A., 2010. A novel fuzzy-sliding mode controller for antilock braking system. In *2nd International Conference on Advanced Computer Control*, Shenyang, China, v. 4, pages 110 – 114.
- Haidegger, T., Kovács, L., Preitl, S., Precup, R.-E., Benyó, B. and Benyó, Z. 2011. Controller design solutions for long distance telesurgical applications. *International Journal of Artificial Intelligence*, 6 (11 S):48 – 71.
- Jing, H., Liu, Z. and Liu, J., 2011. Wheel slip control for hybrid braking system of electric vehicle. In *TMEE'11, International Conference on Transportation, Mechanical, and Electrical Engineering*, Changchun, China, pages 743 – 746.
- Kadowaki, S., Ohishi, K., Hata, T., Iida, N., Takagi, M., Sano, T. and Yasukawa, S. 2007. Antislip adhesion control based on speed sensorless vector control and disturbance observer for electric commuter train AT series 205-5000 of the east Japan railway company. *IEEE Transactions on Industrial Electronics*, 54(4):2001 – 2008.
- Kiyakli, O. and Solmaz, H., 2018. Modeling of an electric vehicle with MATLAB/Simulink. *International Journal of Automotive Science and Technology*, 2(4):9 – 15.
- Li, W., Zhu, X. and Ju, J., 2018. Hierarchical braking torque control of in-wheel-motor-driven electric vehicles over CAN. *IEEE Access*, 6, pages 65189 – 65198.
- Lin, H. and Song, C., 2011. Design of a fuzzy logic controller for ABS of electric vehicle based on AMESim and Simulink. In *TMEE'11, International Conference on Transportation, Mechanical, and Electrical Engineering*, Changchun, China, pages 779 – 782.
- Naseri, F., Farjah, E. and Ghanbari, T., 2017. An efficient regenerative braking system based on battery / supercapacitor for electric, hybrid, and plug-in hybrid electric vehicles with BLDC motor. *IEEE Transactions on Vehicular Technology*, 66(5):3724 – 3738.
- Pacejka, H., 2012. *Tyre and Vehicle Dynamics* (3rd ed.), Oxford, UK: Butterworth-Heinemann.
- Pratap, R. and Ruina, A., 2002. *Introduction to Statics and Dynamics*. Oxford University Press.
- Precup, R.-E., Tomescu, M.-L. and Dragos, C.-A. 2014. Stabilization of Rössler chaotic dynamical system using fuzzy logic control algorithm. *International Journal of General Systems*, 43(5):413 – 433.
- Radgolchin, M. and Moeenfarid, H. 2018. Development of a multi-level adaptive fuzzy controller for beyond pull-in stabilization of electrostatically actuated microplates. *Journal of Vibration and Control*. 24(5):860 – 878.
- Reif, K. (Ed.), 2014. *Brakes, Brake Control and Driver Assistance Systems: Function, Regulation and Components*. Friedrichshafen, Germany: Springer.

- Savaresi, S. M. and Tanelli, M., 2010. *Active Braking Control Systems Design for Vehicles*. London: Springer.
- Shang, M., Chu, L., Guo, J., and Fang, Y., 2010. Hydraulic braking force compensation control for hybrid electric vehicles. In *CMCE'10, International Conference on Computer, Mechatronics, Control and Electronic Engineering*, Changchun, China, pages 335 – 339.
- Spichartz, P., Bokker, T. and Sourkounis, C., 2017. Comparison of electric vehicles with single drive and four wheel drive system concerning regenerative braking. In *EVER'17, 12th International Conference on Ecological Vehicles and Renewable Energies*, Monte-Carlo, Monaco, pages 1 – 7.
- Tao, Y., Xie, X., Zhao, H., Xu, W. and Chen, H., 2017. A regenerative braking system for electric vehicle with four in-wheel motors based on fuzzy control. In *36th Chinese Control Conference*, Dalian, China, pages 4288 – 4293.
- Xie, Y-B. and Wang, S-C, 2018. Research on regenerative braking control strategy and Simulink simulation for 4WD electric vehicle. In *ICMT'18, 2nd International Conference on Manufacturing Technologies*, Florence, USA, pages 1 – 6.
- Xu, W., Zhao, H., Ren, B. and Chen, H., 2016. A regenerative braking control strategy for electric vehicle with four in-wheel motors. In *35th Chinese Control Conference*, Chengdu, China, pages. 8671 – 8676.
- Zhang, X. and Lin, H., 2018. UAV anti-skid braking system simulation. In *37th Chinese Control Conference*, Wuhan, China, pages 8453 – 8458.

